Stability of the flow of a fluid through a flexible tube at high Reynolds number

By V. KUMARAN

Department of Chemical Engineering, Indian Institute of Science, Bangalore 560 012, India

The stability of the Hagen–Poiseuille flow of a Newtonian fluid in a tube of radius R surrounded by an incompressible viscoelastic medium of radius $R < r < HR$ is analysed in the high Reynolds number regime. The dimensionless numbers that affect the fluid flow are the Reynolds number $Re = (\rho VR/\eta)$, the ratio of the viscosities of the wall and fluid $\eta_r = (\eta_s/\eta)$, the ratio of radii H and the dimensionless velocity $\Gamma = (\rho V^2/G)^{1/2}$. Here ρ is the density of the fluid, G is the coefficient of elasticity of the wall and V is the maximum fluid velocity at the centre of the tube. In the high Reynolds number regime, an asymptotic expansion in the small parameter $\epsilon = (1/Re)$ is employed. In the leading approximation, the viscous effects are neglected and there is a balance between the inertial stresses in the fluid and the elastic stresses in the medium. There are multiple solutions for the leading-order growth rate $s^{(0)}$, all of which are imaginary, indicating that the fluctuations are neutrally stable, since there is no viscous dissipation of energy or transfer of energy from the mean flow to the fluctuations due to the Reynolds stress.

There is an $O(\epsilon^{1/2})$ correction to the growth rate, $s^{(1)}$, due to the presence of a wall layer of thickness $\epsilon^{1/2}R$ where the viscous stresses are $O(\epsilon^{1/2})$ smaller than the inertial stresses. An energy balance analysis indicates that the transfer of energy from the mean flow to the fluctuations due to the Reynolds stress in the wall layer is exactly cancelled by an opposite transfer of equal magnitude due to the deformation work done at the interface, and there is no net transfer from the mean flow to the fluctuations. Consequently, the fluctuations are stabilized by the viscous dissipation in the wall layer, and the real part of $s^{(1)}$ is negative. However, there are certain values of Γ and wavenumber k where $s^{(1)} = 0$. At these points, the wall layer amplitude becomes zero because the tangential velocity boundary condition is identically satisfied by the inviscid flow solution. The real part of the $O(\epsilon)$ correction to the growth rate $s^{(2)}$ turns out to be negative at these points, indicating a small stabilizing effect due to the dissipation in the bulk of the fluid and the wall material. It is found that the minimum value of $s^{(2)}$ increases $\propto (H-1)^{-2}$ for $(H-1) \ll 1$ (thickness of wall much less than the tube radius), and decreases $\propto H^{-4}$ for $H \gg 1$. The damping rate for the inviscid modes is smaller than that for the viscous wall and centre modes in a rigid tube, which have been determined previously using a singular perturbation analysis. Therefore, these are the most unstable modes in the flow through a flexible tube.

1. Introduction

Fluid flow in a tube with flexible walls is observed in biological systems, such as the flow of blood and other fluids in the body, and in industrial applications such as hollow fibre reactors and membrane bioreactors. Experimental evidence suggests that the

characteristics of the fluid flow in a flexible tube could be very different from those in a rigid tube, since the dynamics of the wall strongly influences the flow field. Krindel & Silberberg (1979) studied the flow of a Newtonian fluid in a gel-walled tube, and observed that the transition Reynolds number and the drag law are very different from those for a rigid tube. Hansen & Hunston (1974) observed the presence of waves on the surface of a disk coated with an elastic material which was spun in a fluid, and Silberberg (1987) showed that the transition Reynolds number for the appearance of waves was very different from that for the transition in flow past flat plates. In this paper, we study the stability of the fluid in a flexible tube at high Reynolds number. The low Reynolds number flow in this geometry was analysed in an earlier paper (Kumaran 1995). A good understanding of the effect of the wall dynamics on the fluid flow would be useful in predicting the transition to turbulence and the drag force in biological flows, and the mass and heat transfer characteristics of these systems.

The flow of a Newtonian fluid through plane channels has been extensively studied. In the case of a rigid-walled channel, the flow is stable in the absence of inertia because the equations of motion do not explicitly depend on time in this case. In the high Reynolds number limit, one might be inclined to neglect the viscous terms in the momentum equation, but there is a theorem due to Rayleigh (see Lin 1966) which states that neutral or unstable fluctuations can exist in an inviscid parallel flow only if the velocity profile has a point of inflexion. Since plane Couette and Poiseuille flows do not have points of inflexion, the inviscid analysis proves inconclusive and it is necessary to include the effect of viscosity. High Reynolds number analyses including the effect of viscosity were carried out by Tollmien (1929), Schlichting (1933), Wasow (1953), Lin 1945 *a–c*) and others (for a review, see Lin 1966). These studies showed that there are solutions of the complete Navier–Stokes equations which do not reduce to the solutions of the inviscid equations because the viscous stresses are important in an internal critical layer of thickness $O(Re^{-1/3})$ smaller than the thickness of the channel, where Re is the Reynolds number. Owing to the presence of this critical layer, sophisticated asymptotic techniques are necessary for obtaining the stability characteristics. The asymptotic analysis indicates, and numerical computations of the linearized Navier–Stokes equations confirm, that a Poiseuille flow through a channel becomes unstable at a Reynolds number of about 5800, and this instability is called the Tollmien–Schlichting instability.

In a channel with flexible walls, the dynamics of the walls could affect the fluid flow, and there is the possibility of an instability at low Reynolds number. The low Reynolds number Couette flow adjacent to a gel was studied by Kumaran, Fredrickson & Pincus (1994), who found an instability even in the absence of inertia when the velocity was increased beyond a critical value. Instabilities are not usually encountered in the absence of inertia because the equations of motion are not explicitly time dependent, but in the analysis of Kumaran *et al.* (1994) the time dependence entered through the elastic terms in the equations for the wall dynamics. This instability is driven by a discontinuity in the strain rate across the interface, which results in the transport of energy from the mean flow to the fluctuations via the deformation work done by the mean flow at the interface. A similar instability was observed in the flow through a flexible tube at low Reynolds number which was subsequently analysed by the present author (Kumaran 1995).

At high Reynolds number, the Tollmien–Schlichting instability is modified owing to the flexibility of the wall. Moreover, the Rayleigh theorem does not apply in this case because a normal velocity is permitted at the wall, and there are additional types of instabilities that could exist in the absence of viscosity. Benjamin (1959, 1963) and

Landahl (1962) used a simple extension of the linear stability theory of Tollmien (1929), Schlichting (1933) and Lin (1945 *a–c*), and classified the instabilities into three types based on the effect of dissipation on the growth of the waves. Class A refers to Tollmien–Schlichting instabilities modified by the flexibility of the wall, and these are destabilized by dissipation in the wall. Class B instabilities are surface resonance type instabilities which travel close to the free wave speed of the surface, and these are damped by the viscous dissipation. Both Class A and B waves can exist only in a viscous fluid, while the Class C waves, which are not affected by dissipation in the wall, can exist in an inviscid flow and are similar to the Kelvin–Helmholtz or aerodynamic flutter instability. More recent linear stability analyses (Carpenter & Garrad 1985, 1986) have numerically solved the complete Navier–Stokes equations to determine the onset of instability. This involves recasting the equations of motion into a single fourth-order Orr–Sommerfeld equation, and determining its eigenvalues numerically. This task is complicated by the stiffness of the Orr–Sommerfeld equations, and sophisticated numerical techniques are required to overcome the stiffness problems. Carpenter & Garrad (1985, 1986) found it convenient to use a two-fold classification – the Tollmien–Schlichting instability which exists only in the presence of fluid viscosity, and the flow-induced surface instability which can exist in an inviscid flow. The preceding studies concluded that the flexibility of the wall usually stabilizes the flow in the boundary layer and increases the Reynolds number at which transition to turbulence occurs; this is in qualitative agreement with experimental results (see, for example, Riley, Gad el Hak & Metcalfe 1988; Carpenter 1990).

Experimental studies on the flow past a flexible surface were conducted by Hansen & Hunston (1974, 1983). Their apparatus consisted of a disk coated with an elastomer made of polyvinyl chloride plasticol suspended in a tank of a Newtonian fluid (usually water). The disk was rotated with a controlled angular velocity, and the torque required was measured. In addition, the surface of the disk was also visually observed. They found that when the angular velocity was increased beyond a critical value, a standing wave structure appeared on the surface, and the drag force on the disk was greater than that on an identical disk without the compliant surface. Silberberg (1987) reported that the critical value of the angular velocity was proportional to $(Ga^3\rho/4H\eta^2)^{1/2}$, where G is the shear modulus of the material, ρ and η are the density and viscosity of the fluid, and a and H are the radius of the disk and the thickness of the compliant surface respectively. This implies that the elastic nature of the surface does not just modify the instability in the flow past a rigid surface, but induces an instability which is absent in the flow past a rigid surface.

The stability of the flow through a rigid tube is qualitatively different from the flow in a plane channel, because there is no critical layer for axisymmetric perturbations. As a result, there is no possibility of unstable modes in the high Reynolds number regime. In fact, the inviscid equations for the temporal stability in an infinite tube have no solutions, and the asymptotic analysis of Gill (1965) in the high Reynolds number regime considered the spatial stability problem, where the evolution of the spatial growth of a disturbance is studied. The inviscid flow solutions were found to be strongly damped, and of little interest. However, the asymptotic studies of Pekeris (1948), Corcos & Sellars (1959) and Gill (1965) revealed that there are two types of singular perturbation solutions for the inviscid equations, where the vorticity is confined to thin regions near the centre of the tube and at the wall.

There have been many linear stability analyses of the flow in a tube at finite Reynolds number. The majority (Davey & Drazin 1969; Garg & Rouleau 1972; Salwen & Grosch 1972) have reported that the flow is stable to small disturbances at all Reynolds

numbers. Davey & Drazin's numerical result was found to be in good agreement with the high Reynolds number asymptotic solutions. Graebel's (1970) asymptotic analysis gave a critical Reynolds number $Re^{1/3} = 3$, but the author concluded that this critical Reynolds number is too small to match the experimental results. As a consequence, there appears to be a consensus that the flow in a rigid tube is stable to small perturbations, but there may be an instability to perturbations of finite amplitude. This conclusion has been reinforced by experimental evidence which indicates that the flow can be maintained in the laminar regime at Reynolds numbers much higher than the critical value of 2300 if adequate precautions are taken to prevent fluctuations in the system. In experiments, the transition to turbulence is not due to growth of waves of a specific wavelength, but rather to the creation of local intermittent disturbances in the entrance region and at the surface of the pipe. Wygnanski & Champagne (1973) identified two mechanisms of instability – the turbulent slugs which are caused by small disturbances in the wall layer and appear at a Reynolds number of about 3200, and the turbulent puff which is observed at the entrance of the pipe at a Reynolds number of about 2300. For a detailed discussion of the transition to turbulence, see Sreenivasan & Ramshankar (1986).

The flow near a flexible surface is very different from the flow near a rigid surface. The Rayleigh theorem is not valid for the flow in a flexible tube because a non-zero normal velocity is permitted at the wall, and there are non-trivial solutions for the temporal stability problem for an inviscid flow in the flexible case. The low Reynolds number analysis (Kumaran 1995) has revealed the possibility of unstable fluctuations when the fluid velocity is increased beyond a critical value, and it would be of interest to carry out a similar analysis in the high Reynolds number limit. In the present paper, we study the stability of the flow in a flexible tube at high Reynolds number using an asymptotic analysis.

As already mentioned, the earlier asymptotic studies of the flow through a rigid pipe have concentrated on the singular perturbation problem, which involves the presence of viscous layers at the centre or at the wall of the tube. This is because there are no non-trivial solutions for the inviscid flow through a rigid tube at high Reynolds number. In the case of a flexible tube, however, there are non-trivial solutions because a normal velocity is permitted at the wall. Therefore, it is possible to use a regular perturbation analysis to obtain the growth rate of the inviscid modes. In §4, the growth rates of the inviscid modes analysed here are compared with the growth rates of viscous modes in a rigid tube obtained previously by a singular perturbation analysis. The present asymptotic analysis is also different from the triple-deck theory used by Carpenter & Gajjar (1990) for the boundary layer flow past a flexible surface. In both analyses, the viscous correction to the leading-order inviscid flow is significant in a wall layer of thickness $O(Re^{-1/2})$ at the surface, where Re is the Reynolds number based on the mean velocity and the tube radius or boundary layer thickness. However, in the case of a plane surface, the Rayleigh equation for the stream function in an inviscid flow contains a singular point when the fluid velocity is equal to the wave velocity of the perturbations (see, for example, Drazin & Reid 1981). Around this point, it is necessary to include the viscous effects in the leading-order theory, and there is an internal viscous layer of thickness $O(Re^{-1/3})$ around this point. In the cylindrical geometry, however, there is no singularity in the Rayleigh equation for axisymmetric modes, and so it is not necessary to include the inner shear layer in the analysis.

The stability of the flow in a flexible tube is determined using a normal mode analysis in §2. This is a temporal stability analysis, where perturbations in the form of Fourier modes are imposed on the base flow, and their temporal growth rate is determined.
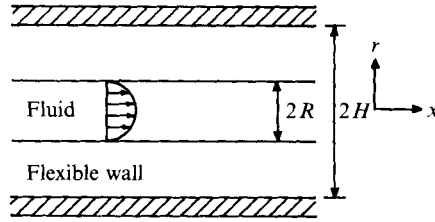
FIGURE 1. Configuration and coordinate system used for the analysis.

This type of analysis has been commonly used in the classical hydrodynamic stability problems. In the study of inviscid shear flows, the initial value analysis (spatial stability analysis) has also been used, where a disturbance in the form of a localized wave packet in space is imposed on the mean flow, and the spatial growth rate of the perturbations is determined. The relationship between the two techniques is given in Drazin & Reid (1981, Chap. 6). When the perturbations are neutrally stable, the spatial and temporal modes coincide because both the spatial and temporal growth rates are imaginary. The normal mode problem is simpler than the initial value problem, and it is possible to obtain analytical results for the growth rate in the former case, whereas the latter involves extensive computation. Since the neutral stability curves are of interest in the present study, it is more convenient to use the normal mode analysis.

The fluid is an incompressible Newtonian fluid, and the wall of the tube is modelled as an incompressible viscoelastic medium in which the stress has an elastic component which depends on the strain field and a viscous component which is proportional to the strain rate. It is of interest to determine the relative magnitudes of the fluid and wall viscosity in a typical application. The time scale for oscillations in the high Reynolds number regime is $t = (\rho R^2/G)^{1/2}$, where ρ is the density of the fluid, R is the radius of the tube and G is the modulus of elasticity. For typical values of $G = 100$ Nm^{-2} for polymer gels, $\rho = 1000$ kg m^{-3} for water and $R = 10^{-3}$ m in biological systems such as blood vessels, the time scale is 3×10^{-3} s. If the imaginary part of the shear modulus G_i is 0.03 times the real part (as is typical for elastic materials), then the solid viscosity $\eta_s = G_i t/3$ is 3×10^{-3}. This is about three times the viscosity of water at room temperature. Therefore, in the present analysis we assume that the viscosities of the solid and fluid are of the same magnitude in the perturbation analysis.

The viscous stresses in the fluid are neglected in the leading-order analysis, and there is a balance between the inertial stresses in the fluid and the elastic stresses in the wall. Since there is no dissipation of energy in the leading approximation, the leading-order growth rate $s^{(0)}$ of the perturbations is imaginary. The viscous stresses are important in a wall layer of thickness $O(Re^{-1/2})$ smaller than the tube radius, and these cause an $O(Re^{-1/2})$ correction $s^{(1)}$ to the growth rate. The real part of the $s^{(1)}$ turns out to be negative in the absence of flow, indicating that the perturbations are stable. However, it is found that $s^{(1)} = 0$ for specific values of the fluid velocity and the wavenumber. At these parameter values, the stability of the flow depends on the $O(Re^{-1})$ correction to the growth rate $s^{(2)}$. The real part of $s^{(2)}$ turns out to be negative, indicating a small stabilizing effect due to the dissipation in the wall and the outer flow.

The reasons for the unusual behaviour of $s^{(1)}$ are further examined using an energy balance analysis in §3. This involves identifying the mechanisms for the transport of energy from the mean flow to the fluctuations and the dissipation of energy. The results of the energy balance analysis are in agreement with those of the linear stability analysis, and provide some physical insight into the energy transfer processes in the flow. The main conclusions are briefly summarized in §4.

2. Linear stability analysis

The system consists of a Newtonian fluid of density ρ and viscosity η flowing through a tube of radius R which is surrounded by an incompressible viscoelastic medium of density ρ, viscosity η_s and coefficient of elasticity G in the annular space $R < r < HR$ as shown in figure 1. In the high Reynolds number limit, it is convenient to scale all lengths by the radius of the tube R, the time coordinate by $(\rho R^2/G)^{1/2}$ and all velocities by $(G/\rho)^{1/2}$. The dimensionless mean flow velocity profile is a Hagen–Poiseuille flow:

$$\bar{v} = \Gamma(1 - r^2), \tag{2.1}$$

where the dimensionless velocity $\Gamma = (\rho V^2/G)^{1/2}$, and V is the maximum fluid velocity. The governing equations for the fluid are the Navier–Stokes mass and momentum equations:

$$\partial_i v_i = 0, \tag{2.2}$$

$$\partial_t v_i + v_j \partial_j v_i = -\partial_i p + \epsilon \Gamma \partial_j^2 v_i, \tag{2.3}$$

where $\partial_t = (\partial/\partial t)$ and $\partial_i = (\partial/\partial x_i)$, $Re = (\rho V R/\eta)$ is the Reynolds number, the pressure in the fluid is non-dimensionalized by the shear modulus G and $\epsilon = (1/Re)$ is a small parameter in the limit $Re \gg 1$. The stress in the fluid is

$$\tau_{ij} = -p\delta_{ij} + \epsilon\Gamma(\partial_i v_j + \partial_j v_i). \tag{2.4}$$

The wall of the tube is modelled using the dynamical equations for an incompressible elastic material (Landau & Lifshitz 1989) modified to include a viscous stress. These equations have been used earlier for polymer gels (Harden, Pleiner & Pincus 1991; Kumaran 1993; Kumaran *et al.* 1994), and for the study of the stability of flow through a flexible tube at low Reynolds number (Kumaran 1995). The dynamics of the wall is described by a displacement field u_i, which represents the displacement of the material points from their steady-state positions due to the stresses at the surface. For an incompressible material, the displacement field u_i satisfies the solenoidal condition

$$\partial_i u_i = 0, \tag{2.5}$$

while the momentum conservation equation is

$$\partial_t^2 u_i = -\partial_i p + \partial_j^2 u_i + \epsilon\Gamma\eta_r \partial_j^2 v_i. \tag{2.6}$$

The left-hand side represents the rate of change of momentum in a volume element, while the three terms on the right-hand side are the divergence of the pressure, the divergence of an elastic stress due to the strain in the material and the divergence of a viscous stress due to the strain rate. In the latter, the velocity is given by $v_i = \partial_t u_i$, and $\eta_r = (\eta_s/\eta)$ is the ratio of the viscosity of the wall material and the fluid. The stress in the wall is given by

$$\sigma_{ij} = -p\delta_{ij} + (\partial_i u_j + \partial_j u_i) + \epsilon\Gamma\eta_r(\partial_i v_j + \partial_j v_i). \tag{2.7}$$

The boundary conditions for the fluid velocity field at the centre of the tube are the symmetry conditions $v_r = 0$ and $\partial_r v_x = 0$, while the wall material is fixed at $r = H$ where the displacement field satisfies $u_r = 0$ and $u_x = 0$. The appropriate boundary conditions at the interface between the fluid and the wall are the continuity of velocity and stress:

$$v_i = \partial_t u_i, \quad \sigma_{ij} = \tau_{ij}. \tag{2.8}$$

In the linear stability analysis, small perturbations in the form of Fourier modes are imposed on the fluid velocity field and the wall displacement field:

$$v_i = \tilde{v}_i \exp{(ikx + st)}, \quad u_i = \tilde{u}_i \exp{(ikx + st)}, \tag{2.9}$$

where k is the wavenumber and s is the growth rate of the perturbations. Upon inserting the above perturbations into the conservation equations for the fluid velocity field ((2.2) and (2.3)), the following equations for the eigenfunctions $\tilde{v}_i$ are obtained for axisymmetric perturbations:

$$(\partial_r + r^{-1})\tilde{v}_r + ik\tilde{v}_x = 0, \tag{2.10}$$

$$[s + \Gamma ik(1 - r^2)]\tilde{v}_r = -\partial_r \tilde{p} + \epsilon\Gamma(\partial_r^2 + r^{-1}\partial_r - r^{-2} - k^2)\tilde{v}_r, \tag{2.11}$$

$$[s + \Gamma ik(1 - r^2)]\tilde{v}_x - 2\Gamma r\tilde{v}_r = -ik\tilde{p} + \epsilon\Gamma(\partial_r^2 + r^{-1}\partial_r - k^2)\tilde{v}_x, \tag{2.12}$$

where $\tilde{p}$ is the eigenfunction for the pressure.

The equations for the eigenfunctions $\tilde{u}_i$ can be obtained by inserting the equation for the perturbation to the displacement field (2.9) into the conservation equations (2.5) and (2.6):

$$(\partial_r + r^{-1})\tilde{u}_r + ik\tilde{u}_x = 0, \tag{2.13}$$

$$s^2\tilde{u}_r = -\partial_r \tilde{p} + [1 + \epsilon\Gamma\eta_r s](\partial_r^2 + r^{-1}\partial_r - r^{-2} - k^2)\tilde{u}_r, \tag{2.14}$$

$$s^2\tilde{u}_x = -ik\tilde{p} + [1 + \epsilon\Gamma\eta_r s](\partial_r^2 + r^{-1}\partial_r - k^2)\tilde{u}_x. \tag{2.15}$$

The boundary conditions at the centre of the tube ($r = 0$) are the symmetry conditions ($\tilde{v}_r = 0$ and $\partial_r\tilde{v}_x = 0$), and the boundary conditions at the surface $r = H$ are the zero displacement conditions ($\tilde{u}_r = 0$ and $\tilde{u}_x = 0$). At the interface $r = 1$, the continuity of velocity and stress conditions are

$$\tilde{v}_r = s\tilde{u}_r, \quad \tilde{v}_x - 2\Gamma\tilde{u}_r = s\tilde{u}_x, \tag{2.16}$$

$$\tilde{\sigma}_{rr} = \tilde{\tau}_{rr}, \quad \tilde{\sigma}_{xr} = \tilde{\tau}_{xr}. \tag{2.17}$$

The second term on the left-hand side of the boundary condition for the tangential velocity (2.16) represents the variation in the mean velocity at the surface due to the surface displacement. This is caused by the discontinuity in the strain rate across the surface in the base state.

In the high Reynolds number limit, the viscous terms in the momentum equations for the fluid ((2.11) and (2.12)) are $O(\epsilon)$ smaller than the inertial terms, and an asymptotic analysis in the small parameter ϵ is suitable. The fluid velocity field can be divided into two regions – an outer flow velocity $\tilde{v}_{oi}$ which is inviscid in the leading-order approximation, and a wall layer velocity $\tilde{v}_{wi}$ where the viscous stresses are important:

$$\tilde{v}_i = \tilde{v}_{oi} + \tilde{v}_{wi}. \tag{2.18}$$

Further analysis indicates that the first correction to the velocity and displacement fields are $O(\epsilon^{1/2})$ smaller than the leading-order terms, and so these quantities are expanded in an asymptotic series as follows:

$$\tilde{v}_{oi} = \tilde{v}_{oi}^{(0)} + \epsilon^{1/2}\tilde{v}_{oi}^{(1)} + \dots, \quad \tilde{u}_i = \tilde{u}_i^{(0)} + \epsilon^{1/2}\tilde{u}_i^{(1)} + \dots, \quad s = s^{(0)} + \epsilon^{1/2}s^{(1)} + \dots. \tag{2.9}$$

In the leading-order approximation for the outer velocity $\tilde{v}_{oi}$, the viscous terms in the fluid momentum conservation equations can be neglected, and the mass and momentum equations ((2.10), (2.11) and (2.12)) can be combined to give the following equation for $\tilde{v}_{or}^{(0)}$:

$$[s^{(0)} + \Gamma ik(1 - r^2)](\partial_r^2 + r^{-1}\partial_r - r^{-2} - k^2)\tilde{v}_{or}^{(0)} = 0. \tag{2.20}$$

The eigenfunctions for the fluid velocity field $\tilde{v}_{or}^{(0)}$ and $\tilde{v}_{ox}^{(0)}$ and pressure field $\tilde{p}^{(0)}$ can be easily obtained by solving the above equation and using (2.10) and (2.12):

$$\tilde{v}_{or}^{(0)} = A_1 I_1(kr), \tag{2.21}$$

$$\tilde{v}_{ox}^{(0)} = iA_1 I_0(kr), \tag{2.22}$$

$$\tilde{p}^{(0)} = (A_1/k)[-(s^{(0)} + \Gamma ik(1 - r^2))I_0(kr) - 2i\Gamma rI_1(kr)], \tag{2.23}$$

where I_0 and I_1 are modified Bessel functions, and A_1 is a constant that has to be determined from the boundary conditions. In the above solutions, the coefficients of the solutions proportional to K_0 and K_1 have been set to zero, as required by the symmetry conditions at $r = 0$.

The equation for the first-order correction to the velocity field, analogous to (2.20), is

$$[s^{(0)} + \Gamma ik(1-r^2)](\partial_r^2 + r^{-1}\partial_r - r^{-2} - k^2)\,\tilde{v}_{or}^{(1)} + s^{(1)}(\partial_r^2 + r^{-1}\partial_r - r^{-2} - k^2)\,\tilde{v}_{or}^{(0)} = 0. \tag{2.24}$$

It can be easily verified that the solution for the first correction to the velocity field is identical to the leading-order velocity field, and therefore we can set $\tilde{v}_{or}^{(1)} = 0$ without loss of generality. With this, the solution for the first correction to the velocity and pressure fields are

$$\tilde{v}_{or}^{(1)} = 0, \quad \tilde{v}_{ox}^{(1)} = 0, \tag{2.25}$$

$$\tilde{p}^{(1)} = -(s^{(1)}/k)\,I_0(kr). \tag{2.26}$$

There is a wall layer of thickness $(\epsilon^{1/2}R)$ at the interface, and the equation for the velocity profile in the wall layer can be obtained by rescaling the radial coordinate $(1-r) = \epsilon^{1/2}y$ in the momentum equations (2.10), (2.11) and (2.12). In turns out that the leading-order wall layer velocities, $\tilde{v}_{wx}^{(0)}$ and $\tilde{v}_{wr}^{(0)}$, are sufficient for the present analysis, and therefore we can remove the superscript (0) for the wall layer velocity. The modified momentum conservation equations, correct to leading order in small ϵ, are

$$-\epsilon^{-1/2}\partial_y\tilde{v}_{wr} + ik\tilde{v}_{wx} = 0, \tag{2.27}$$

$$-\epsilon^{-1/2}\partial_y\tilde{p} + (-s^{(0)} + \Gamma\partial_y^2)\tilde{v}_{wr} = 0, \tag{2.28}$$

$$-ik\tilde{p} + (-s^{(0)} + \Gamma\partial_y^2)\tilde{v}_{wx} = 0. \tag{2.29}$$

The above equations can easily be solved to obtain the following velocity profile in the wall layer:

$$\tilde{v}_{wx} = A_i\exp(-y(s^{(0)}/\Gamma)^{1/2}), \tag{2.30}$$

$$\tilde{v}_{wr} = -A_i ik(\epsilon\Gamma/s^{(0)})^{1/2}\exp(-y(s^{(0)}/\Gamma)^{1/2}), \tag{2.31}$$

where the amplitude A_i is determined from the boundary condition for the tangential velocity. The above solutions are consistent for both upstream and downstream travelling waves, because if $s^{(0)}$ is expressed as $|s^{(0)}|\exp(i\theta)$, where the θ is chosen such that $0 < \theta < \pi$ for upstream waves and $-\pi < \theta < 0$ for downstream waves, then the real part of $s^{(0)^{1/2}}$ is always positive. For future reference, the shear stress in the wall layer is

$$\tilde{\tau}_{wxr} = \epsilon^{1/2}A_i(\Gamma s^{(0)})^{1/2}\exp(-y(s^{(0)}/\Gamma)^{1/2}). \tag{2.32}$$

The eigenfunctions for the displacement field in the wall material are determined next. The leading-order eigenfunctions for the displacement field, obtained by solving (2.13), (2.14) and (2.15) are

$$\tilde{u}_r^{(0)} = B_1 K_1(\gamma r) + B_2 K_1(kr) + B_3 I_1(\gamma r) + B_4 I_1(kr), \tag{2.33}$$

$$\tilde{u}_x^{(0)} = -(iB_1\gamma/k)K_0(\gamma r) - iB_2 K_0(kr) + (iB_3\gamma/k)I_0(\gamma r) + iB_4 I_0(kr), \tag{2.34}$$

$$\tilde{p}^{(0)} = B_2(\gamma^2/k - k)K_0(kr) - B_4(\gamma^2/k - k)I_0(kr), \tag{2.35}$$

where $\gamma = [k^2 + (s^{(0)})^2]^{1/2}$ and K_0 and K_1 are modified Bessel functions. The constants, B_1, B_2, B_3 and B_4 are determined from the zero displacement conditions at $r = H$, and the velocity and stress conditions at the interface ((2.16) and (2.17)). The first

corrections to the displacement fields, $\tilde{u}_r^{(1)}$ and $\tilde{u}_x^{(1)}$, evaluated from (2.13), (2.14) and (2.15) are

$$\tilde{u}_r^{(1)} = -B_1(s^{(0)}s^{(1)}r/\gamma)\,K_0(\gamma r) + B_3(s^{(0)}s^{(1)}r/\gamma)\,I_0(\gamma r), \qquad (2.36)$$

$$\tilde{u}_x^{(1)} = -B_1\left(\frac{\mathrm{i}s^{(0)}s^{(1)}}{\gamma k}\right)[2K_0(\gamma r) - \gamma r K_1(\gamma r)] + B_3\left(\frac{\mathrm{i}s^{(0)}s^{(1)}}{\gamma k}\right)[2I_0(\gamma r) + \gamma r I_1(\gamma r)]. \quad (2.37)$$

The leading-order velocity and stress boundary conditions at the interface $r = 1$ ((2.16) and (2.17)) are

$$\tilde{v}_{or}^{(0)} = s^{(0)}\tilde{u}_r^{(0)}, \quad \tilde{v}_{ox}^{(0)} + \tilde{v}_{wx} - 2\Gamma\tilde{u}_r^{(0)} = s^{(0)}u_x^{(0)}, \qquad (2.38)$$

$$\tilde{\tau}_{orr}^{(0)} = \tilde{\sigma}_{rr}^{(0)}, \quad \tilde{\sigma}_{xr}^{(0)} = 0. \qquad (2.39)$$

The normal velocity in the wall layer $\tilde{v}_{wr}$ does not enter the leading-order boundary conditions because it is $O(\epsilon^{1/2})$ smaller than the tangential velocity $\tilde{v}_{wx}$. The shear stress in the outer flow $\tilde{\tau}_{xr}$ (2.4) is $O(\epsilon)$ smaller than the shear stress in the wall $\tilde{\sigma}_{xr}$ (2.7), and so the former has been neglected in the stress balance condition (2.39). Similarly, it can easily be verified that the normal and shear stresses in the wall layer, $\tilde{\tau}_{wrr}$ and $\tilde{\tau}_{wxr}$, are $O(\epsilon)$ and $O(\epsilon^{1/2})$ smaller than the respective stresses in the wall material, and so these are also neglected in the stress balance conditions. The velocity and pressure fields in the fluid, (2.21), (2.22) and (2.23), the velocity in the wall layer, (2.30) and (2.31), and the displacement and pressure fields in the wall, (2.33), (2.34) and (2.35), are inserted into the boundary conditions (2.38) and (2.39) and solved to obtain the characteristic equation for the growth rate $s^{(0)}$. From (2.38) and (2.39), it can be seen that boundary conditions for the normal velocity, $\tilde{v}_{or}^{(0)}$, and normal and shear stresses, $\tilde{\sigma}_{rr}^{(0)}$ and $\tilde{\sigma}_{xr}^{(0)}$, are independent of the wall layer velocity $\tilde{v}_{wx}$, so these three can be solved independently to determine the growth rate $s^{(0)}$. With this simplification, the characteristic matrix for the leading-order displacement field is the following 5×5 matrix:

$$\begin{vmatrix} s^{(0)}K_1(\gamma) & s^{(0)}K_1(k) & s^{(0)}I_1(\gamma) \\[4pt] -\gamma[K_0(\gamma) + K_2(\gamma)] & \dfrac{-\gamma^2}{k}K_0(k) - kK_2(k) & \gamma[I_0(\gamma) + I_2(\gamma)] \\[4pt] \dfrac{\mathrm{i}(\gamma^2 + k^2)}{k}K_1(\gamma) & 2\mathrm{i}kK_1(k) & \dfrac{\mathrm{i}(\gamma^2 + k^2)}{k}I_1(\gamma) \\[4pt] K_1(\gamma H) & K_1(kH) & I_1(\gamma H) \\[4pt] \dfrac{-\mathrm{i}\gamma}{k}K_0(\gamma H) & -\mathrm{i}K_0(kH) & \dfrac{\mathrm{i}\gamma}{k}I_0(\gamma H) \end{vmatrix}$$

$$\begin{vmatrix} s^{(0)}I_1(k) & I_1(k) \\[4pt] \dfrac{\gamma^2}{k}I_0(k) + kI_2(k) & \dfrac{s^{(0)}}{k}I_0(k) + \dfrac{2\mathrm{i}\Gamma}{k}I_1(k) \\[4pt] 2\mathrm{i}kI_1(k) & 0 \\[4pt] I_1(kH) & 0 \\[4pt] \mathrm{i}I_0(kH) & 0 \end{vmatrix}. \qquad (2.40)$$

In the above matrix, the first row represents the normal velocity boundary condition (2.38), the second and third rows are the normal and tangential stress conditions (2.39), and the fourth and fifth rows are a consequence of the zero displacement conditions at $r = H$. The growth rate $s^{(0)}$ is determined by solving the characteristic equation Det($\boldsymbol{M}$) $= 0$, and the amplitude of the wall layer velocity, A_i, can then be determined from the boundary condition for the tangential velocity $\tilde{v}_{ox}^{(0)}$ (2.38).

The characteristic equation admits multiple solutions for the growth rate $s^{(0)}$, all of which are imaginary, indicating that the perturbations are neutrally stable in the leading-order approximation. In the absence of fluid flow, the frequency ω, which is the
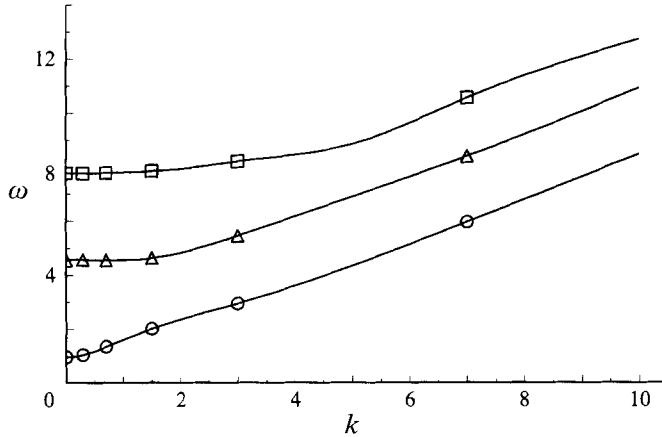
V. Kumaran

FIGURE 2. Leading-order frequency ω as a function of the wavenumber k at $\Gamma = 0$ for $H = 2$. ◯, First harmonic; △, second harmonic; ▢, third harmonic.
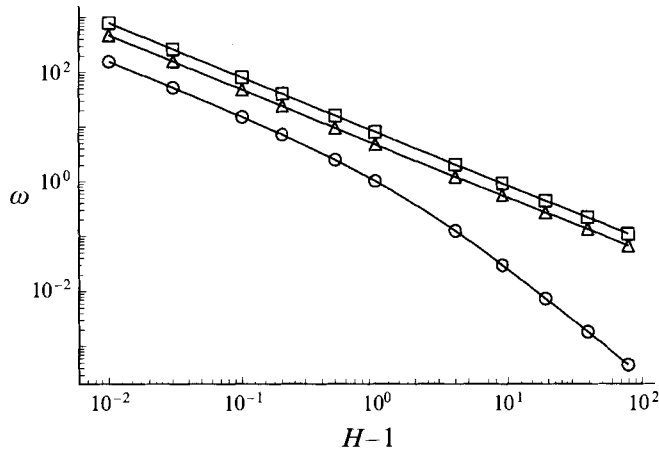

FIGURE 3. The frequency ω as a function of H in the limit $k \to 0$. ◯, First harmonic; △, second harmonic; ▢, third harmonic.

imaginary part of $s^{(0)}$, has solutions that are equal in magnitude and opposite in sign. The magnitudes of the first three harmonics for ω as a function of the wavenumber k for $H = 2$ are shown in figure 2. The frequency has a finite value in the limit $k \to 0$, and increases proportional to k for $k \gg 1$. The limiting values of ω for $k = 0$ are shown as a function of H in figure 3. In the limit $(H-1) \ll 1$, which corresponds to a planar viscoelastic medium in contact with an infinite fluid, the frequency has an infinite number of solutions $[(\pi/2)(H-1)^{-1}], [(3\pi/2)(H-1)^{-1}], \ldots$. These values are consistent with those reported earlier (Kumaran 1993) for the frequencies of the surface modes on a planar viscoelastic medium of finite thickness, and serve as a consistency check for the present calculation. In the limit $H \gg 1$, the value of the lowest harmonic decays proportional to H^{-2}, while the higher harmonics decay as H^{-1}.

It is useful to consider the physical reason for the presence of an infinite number of solutions for the frequency. Multiple harmonics are usually associated with an oscillatory variation in the eigenfunction for the velocity or displacement fields. From (2.21) and (2.22) for the outer velocity field, it can be seen that the outer velocity increases monotonically from the centre to the wall of the tube. This is due to the
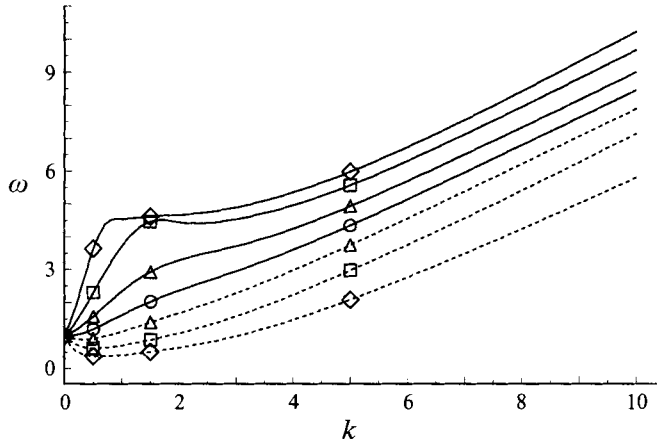
FIGURE 4. Effect of variation in Γ on the frequency ω of the fluctuations for the first harmonic for $H = 2$. The solid lines represent downstream travelling waves ($\omega < 0$), and the broken lines represent upstream travelling waves ($\omega > 0$). $\bigcirc$, $\Gamma = 0$; $\triangle$, $\Gamma = 2$; $\square$, $\Gamma = 5$; $\diamondsuit$, $\Gamma = 10$.

absence of elasticity in the fluid, which is necessary to sustain oscillatory behaviour. The multiple harmonics are due to the oscillatory variation in the displacement field as a function of radius in (2.33) and (2.34), and the number of oscillations increases by one for each successively higher harmonic. Therefore, the presence of multiple harmonics is essentially due to the wall dynamics. Multiple harmonics could be present even in the absence of fluid, as illustrated in Kumaran (1993).

The modification of the frequency due to a fluid flow for the first harmonic is shown in figure 4; the higher harmonics exhibit similar behaviour. An increase in the fluid velocity tends to increase the frequency of waves with $\omega < 0$ (downstream travelling waves), and decrease the frequency of waves with $\omega > 0$ (upstream travelling waves).

The leading-order calculation has proved inconclusive in determining the stability of the perturbations, and it is now necessary to determine the $O(\epsilon^{1/2})$ correction to the growth rate $s^{(1)}$ by solving the $O(\epsilon^{1/2})$ correction to the characteristic matrix $\boldsymbol{M}$. For this, it is necessary to determine the $O(\epsilon^{1/2})$ correction to the displacement field in the wall material (2.36) and (2.37), and the corresponding stresses, and the wall layer velocity (2.30) and (2.31) and the corresponding fluid stresses. The calculation is fairly simple but tedious, and the details are not given here. It is sufficient to note that the magnitudes of the real and imaginary parts of $s^{(1)}$ are equal. This is because the inhomogeneous terms in the equations for the $O(\epsilon^{1/2})$ velocity and stress conditions are the normal velocity and shear stress at the surface, which are proportional to $1/(s^{(0)})^{1/2}$ and $(s^{(0)})^{1/2}$ respectively (see (2.31) and (2.32)). Also, the first correction to the displacement field $\tilde{u}_r^{(1)}$ and $\tilde{u}_x^{(1)}$ ((2.36) and (2.37)) is independent of the viscosity of the wall material η_r, and therefore $s^{(1)}$ is also independent of η_r.

It is more convenient to consider the product $(s^{(1)}/\Gamma^{1/2})$ instead of $s^{(1)}$ itself while discussing the results, because $(s^{(1)}/\Gamma^{1/2})$ remains finite in the limit $\Gamma \to 0$, whereas $s^{(1)}$ becomes small as $\Gamma^{1/2}$. This smallness of $s^{(1)}$ is an artifact of the asymptotic analysis, however, because the limit $\Gamma \to 0$ implies $V \to 0$, and in this limit the parameter $\epsilon \sim (1/V)$ is no longer small. However, the ratio $\Gamma\epsilon$ remains finite in this limit since it is independent of the velocity, and so the first correction to the growth rate scaled by $(\Gamma\epsilon)^{1/2}$ remains finite. Moreover, $(s^{(1)}/\Gamma^{1/2})$ is independent of the fluid velocity, whereas $s^{(1)}$ itself depends on the fluid velocity owing to the dependence of ϵ on V, and so $(s^{(1)}/\Gamma^{1/2})$ is a better measure of the absolute growth rate of the fluctuations. For the
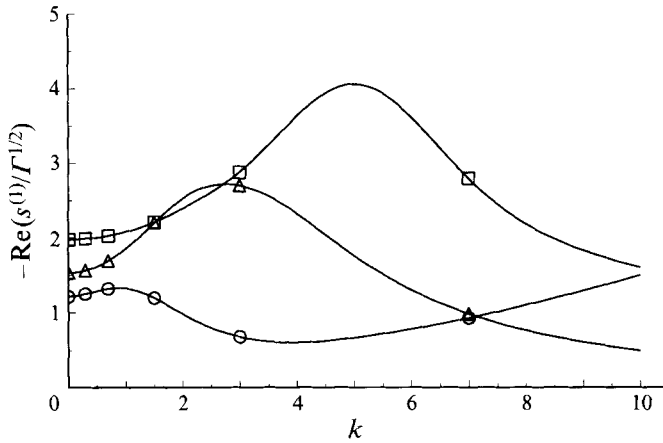
FIGURE 5. The real part of $(s^{(1)}/\Gamma^{1/2})$, as a function of k for $H = 2$ and $\Gamma = 0$. $\bigcirc$, First harmonic; $\triangle$, second harmonic; $\square$, third harmonic.
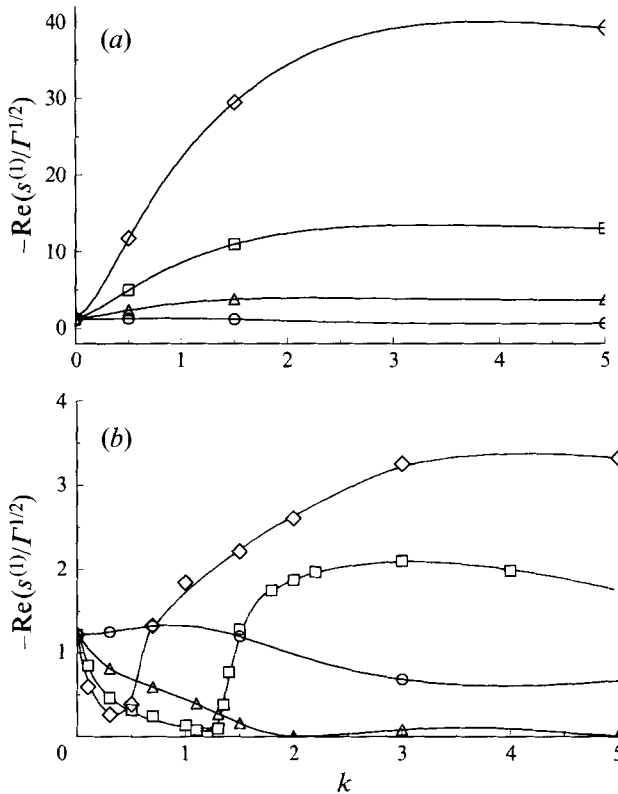

FIGURE 6. Effect of variation in Γ on the real part of $(s^{(1)}/\Gamma^{1/2})$ of (a) upstream travelling waves $\omega > 0$ and (b) downstream travelling waves $\omega < 0$, for the first harmonic for $H = 2$. $\bigcirc$, $\Gamma = 0$; $\triangle$, $\Gamma = 2$; $\square$, $\Gamma = 5$; $\diamondsuit$, $\Gamma = 10$.

same reasons, it will also be convenient to plot $(s^{(2)}/\Gamma)$ rather than the second correction to the growth rate $s^{(2)}$ itself later in the analysis.

The variation in the real part of $s^{(1)}$ in the absence of fluid flow for the first three harmonics is shown in figure 5. It can be seen that $s^{(1)}$ is always negative, indicating that
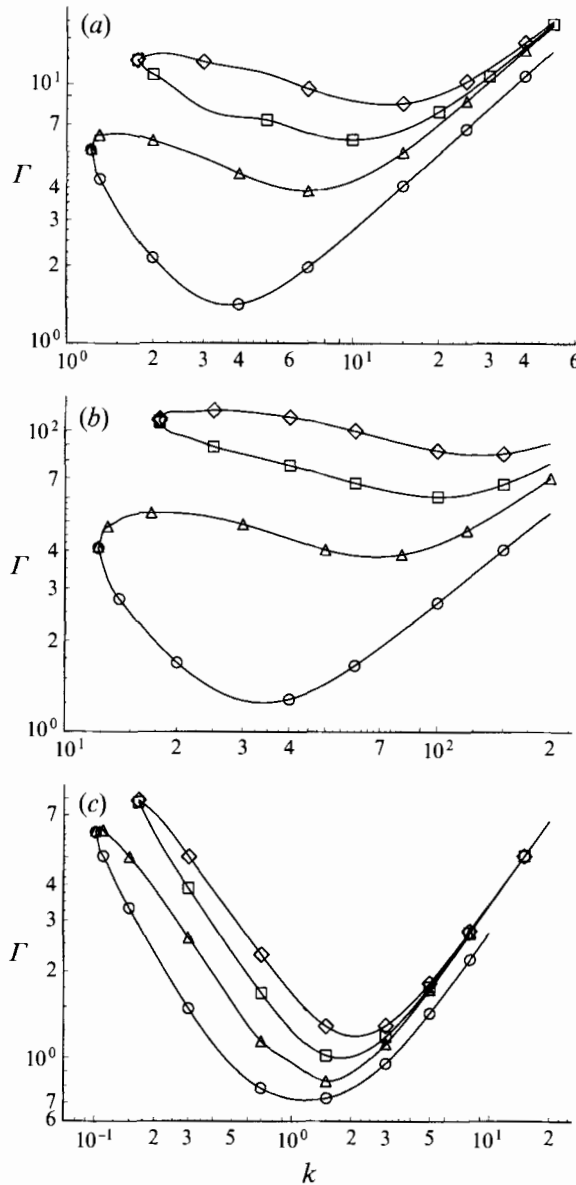
FIGURE 7. Locus of points in Γ, k space where $s^{(1)} = 0$ for (a) $H = 2$, (b) $H = 1.1$ and c) $H = 10$. $\bigcirc$, First harmonic; $\triangle$, second harmonic; $\square$, third harmonic; $\diamond$, fourth harmonic.

the waves are stable. It is interesting to note that for the first harmonic, $s^{(1)}$ increases $\propto k^{3/2}$ for $k \gg 1$, while for the higher harmonics $s^{(1)}$ decreases proportional to $k^{3/2}$ in the same limit. This difference in behaviour will be briefly discussed at the end of the next section.

The effect of fluid flow tends to increase the magnitude of $s^{(1)}$ for the upstream travelling waves ($\omega > 0$), as shown in figure 6(a), thereby stabilizing the perturbations. An increase in the fluid velocity has the opposite effect for the downstream travelling waves ($\omega < 0$), as shown in figure 6(b). In addition, we see that $s^{(1)}$ decreases to zero for specific values of $\Gamma = \Gamma_c$ and $k = k_c$, indicating that perturbations are neutrally
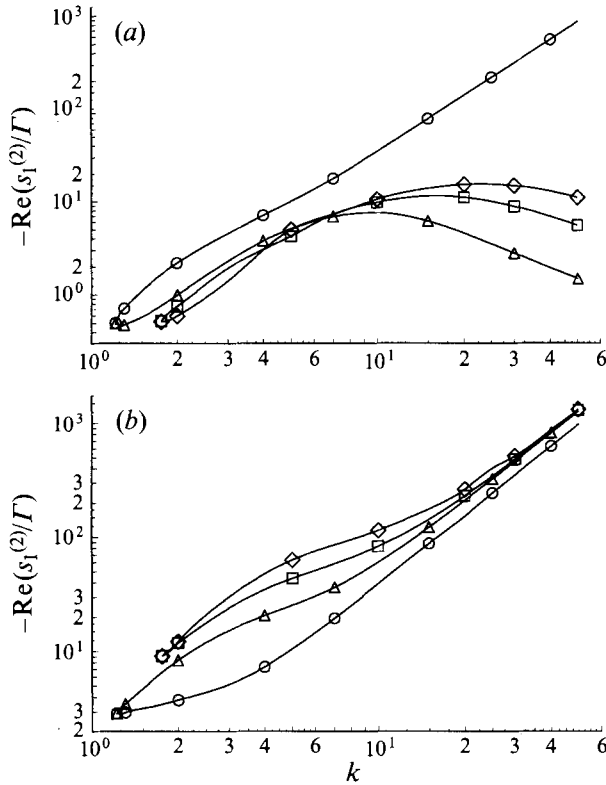
FIGURE 8. The real parts of (a) $(s_1^{(2)}/\Gamma)$ and (b) $(s_2^{(2)}/\Gamma)$ along the points in Γ, k space where $s^{(1)} = 0$ for $H = 2$. $\bigcirc$, First harmonic; $\triangle$, second harmonic; $\square$, third harmonic; $\diamond$, fourth harmonic.

stable at this level of approximation as well. The locus of the points (Γ_c, k_c) where $s^{(1)} = 0$ is shown for the first four harmonics in figure 7(a) for $H = 2$. This feature is observed even at other values of H, as shown in figure 7(b) for $H = 1.1$ and figure 7(c) for $H = 10$. The present calculations also reveal that at the critical points (Γ_c, k_c), the velocity in the wall layer $\tilde{v}_{wx}$ is identically zero. The physical reason for the presence of parameter values with $s^{(1)} = 0$ and $\tilde{v}_{wx} = 0$ will be discussed in detail in the energy balance analysis. The higher-order upstream modes up to the fourth order were also studied and it was found that the fluid flow has a stabilizing effect on these perturbations. For these modes, there were no parameter values where the first correction to the growth rate $s^{(1)}$ decreased to zero.

In the neighbourhood of the points (Γ_c, k_c), $s^{(1)}$ decreases proportional to $(k - k_c)^2$. Therefore, in a region of width $\epsilon^{1/4}$ about the points (Γ_c, k_c) the decay rate of the fluctuations is determined by the second correction $s^{(2)}$. The procedure for calculating this is similar to that for $s^{(1)}$, but it is necessary to include the viscous stresses in the outer flow and the wall material. In addition, the calculation can be greatly simplified by setting the wall layer amplitude equal to zero while determining $s^{(2)}$, the error due to this approximation is $O(\epsilon^{1/4})$. The $O(\epsilon)$ growth rate $s^{(2)}$ is now dependent on η_r, since the dissipation in the wall material is included, and has the form $s^{(2)} = s_1^{(2)} + \eta_r s_2^{(2)}$. The values of the real parts of $(s_1^{(2)}/\Gamma)$ and $(s_2^{(2)}/\Gamma)$ are shown as a function of k for the first four harmonics in figures 8(a) and 8(b) for the parameter values where $s^{(1)} = 0$. The qualitative behaviour of $s^{(2)}$ is similar for other values of H. The real parts of $s_1^{(2)}$ and $s_2^{(2)}$ are negative, indicating that the $O(\epsilon)$ correction to the growth rate has a small
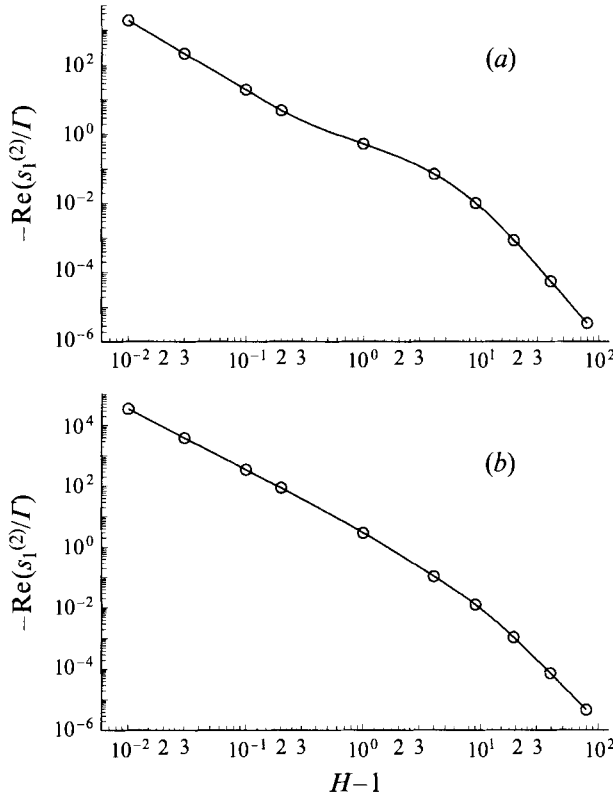
FIGURE 9. The minimum value of the real parts of (a) $(s_1^{(2)}/\Gamma)$ and (b) $(s_2^{(2)}/\Gamma)$ for the lowest harmonic as a function of H.

stabilizing effect on the fluctuations. In figure 8(a), the reason for difference in the qualitative behaviour of $s_1^{(2)}$ for the first and higher harmonics in the limit $k \gg 1$ is similar to the reason for the behaviour of $s^{(1)}$ in this limit. In figure 8(b), the decay rate due to the dissipation in the viscoelastic medium, $s_2^{(2)}$, shows a monotonic increase, and diverges proportional to k^2 for large k. In addition, it can be seen that $s_1^{(2)}$ and $s_2^{(2)}$ increase as the frequency of the harmonics increases, except for the decrease in $s_1^{(2)}$ from the first to second harmonic at large k mentioned above.

It is of interest to examine the variation in the minimum of $s^{(2)}$ with H, since this represents the slowest decay rate of the fluctuations. The minimum value of $s^{(2)}$ would, in general, depend on η_r because $s_1^{(2)}$ decreases and $s_2^{(2)}$ increases in the limit $k \gg 1$ for the second and higher harmonics. However, for $\eta_r \sim O(1)$, we would expect the minimum value of $s^{(2)}$ to coincide with the minimum value of $s_2^{(2)}$ owing to the sharp increase in $s_2^{(2)}$ at large k. The minimum values of $(s_1^{(2)}/\Gamma)$ and $(s_2^{(2)}/\Gamma)$ for the lowest harmonic are shown as a function of H in figures 9(a) and 9(b). This figure shows that $s_1^{(2)}$ and $s_2^{(2)}$ increase proportional to $(H-1)^{-2}$ for $(H-1) \ll 1$, and show a sharp decrease proportional to H^{-4} for $H \gg 1$.

To symmarize, the salient conclusions at this point are the following.

(i) The leading-order growth rate $s^{(0)}$ is imaginary, so the waves are neutrally stable in the leading approximation.

(ii) The first correction $s^{(1)}$ is negative for upstream travelling waves, but $s^{(1)}$ can attain the value of zero for downstream travelling waves at specific critical values (Γ_c, k_c).

(iii) At these critical points, the second correction to the growth rate, $s^{(2)}$, could stabilize or destabilize the waves. The present calculations show that there are two contributions to $s^{(2)}$ – one due to the viscosity in the fluid and the other due to the wall viscosity. Both of these turn out to have a stabilizing effect on the fluctuations. The physical reason for this type of behaviour will be discussed in the next section.

Finally, it is important to note that in the above analysis, we have considered the ratio of solid and fluid viscosities $\eta_r \sim O(1)$. For some solids, this ratio could be large, and the dissipation due to the solid viscosity will be of the same magnitude as the dissipation in the fluid for $\eta_r \sim O(\epsilon^{-1/2})$. For these solids, the additional contribution to $s^{(1)}$ due to the solid damping is given by $\eta_r \epsilon^{-1/2} s_2^{(2)}$, where $s_2^{(2)}$ is calculated as shown above, and given in figure 9(b). In this case, the $O(\epsilon^{1/2})$ correction to the growth rate itself is negative, and there will not be any parameter values where the fluctuations are neutrally stable.

3. Energy balance calculation

The analysis of the previous section has shown that the qualitative behaviour of the decay of fluctuations is different from that reported previously in literature for the flow in a rigid tube. In particular, the decay rate of the fluctuations is $O(\epsilon^{1/2})$ smaller than the leading-order frequency, except along certain lines in the Γ, k parameter space where the decay is $O(\epsilon)$ smaller than the leading-order frequency. In addition, the behaviour of the first correction to the growth rate, $s^{(1)}$, for the first harmonic is qualitatively different from that for higher harmonics. In the present section, an energy balance analysis is used to examine the reasons for this unusual behaviour.

The total energy balance for the fluctuations in the fluid and the viscoelastic medium can be written in the following simple form (Chandrasekhar 1981):

$$\partial_t \mathscr{E} = \mathscr{C} + \mathscr{S} - \mathscr{D}, \tag{3.1}$$

where $\mathscr{E}$ is the total energy of the fluctuations, $\mathscr{C}$ is the rate of increase of energy due to the convective terms in the momentum conservation equation, $\mathscr{S}$ is the rate of increase of energy due to the deformation work done by the stresses at the bounding surfaces of the fluid and the solid and $\mathscr{D}$ is the rate of dissipation of energy. It is important to note that $\mathscr{E}$ in (3.1) refers to the sum of the fluctuation energies in the solid and fluid, and we do not write separate equations for the solid and fluid phases. The total energy is the sum of the kinetic energy of motion of the fluid and the wall and the elastic strain energy:

$$\mathscr{E} = \frac{1}{2} \int dx \int_0^H r \, dr (v_r^2 + v_x^2)$$

$$+ \frac{1}{2} \int dx \int_1^H r \, dr [(\partial_r u_r)^2 + (\partial_x u_x)^2 + \tfrac{1}{2}(\partial_r u_x + \partial_x u_r)^2]$$

$$= (2\pi)^{-1} \exp[(s + s^*) t] \int dk \mathscr{E}(k). \tag{3.2}$$

Here, the energy $\mathscr{E}$ has been non-dimensionalized by GR^3, and the energy spectrum, $\mathscr{E}(k)$, represents the energy in fluctuations with wavenumber k. From the above equation, the rate of change of energy is proportional to the real part of the growth rate. An asymptotic expansion is used for the rate of change of energy:

$$\partial_t \mathscr{E}(k) = 2Re(s^{(0)})\mathscr{E}^{(0)}(k) + 2\epsilon^{1/2} Re(s^{(1)})\mathscr{E}^{(1)}(k), \tag{3.3}$$

where $\partial_t \mathscr{E}(k)$ has been non-dimensionalized by $(G^3 R^6/\rho)^{1/2}$, and $\mathscr{E}^{(0)}$ and $\mathscr{E}^{(1)}$ have been scaled by (GR^4).

The rate of dissipation of energy in the fluid (Chandrasekhar 1981) is

$$\mathscr{D} = \tfrac{1}{2}\Gamma\epsilon \int dx \int_0^1 r\, dr[4(\partial_r v_r)^2 + 4(\partial_x v_x)^2 + 2(\partial_r v_x + \partial_x v_r)^2]. \tag{3.4}$$

The factor $\Gamma\epsilon$ is present in the above equation because the dissipation rate is proportional to the viscosity η. The dissipation in the solid is given by

$$\mathscr{D} = \Gamma\epsilon\eta_r \int dx \int_1^H r\, dr[4(\partial_r v_r)^2 + 4(\partial_x v_x)^2 + 2(\partial_r v_x + \partial_x v_r)^2]. \tag{3.5}$$

It is useful to estimate the magnitudes of the dissipation rates in the fluid and the solid. In the outer flow, the length scale of the fluctuations is $O(R)$, while the velocity scales as $(G/\rho)^{1/2}\tilde{v}$, where $\tilde{v}$ is the dimensionless amplitude of perturbations. Using these, it can be seen that the rate of dissipation scales as $(G\eta R/\rho)\tilde{v}^2 \equiv \Gamma\epsilon(G^3 R^4/\rho)^{1/2}\tilde{v}^2$. A similar argument can be used to show that in the solid, the rate of dissipation scales as $\Gamma\epsilon\eta_r(G^3 R^4/\rho)^{1/2}\tilde{v}^2$. In the viscous wall layer in the fluid, however, the length scale for the variation of the velocity scales as $\epsilon^{1/2}R$, and it can be easily verified from (3.4) that the rate of dissipation of energy is $O(\Gamma\epsilon^{1/2}(G^3 R^4/\rho)^{1/2}\tilde{v}^2)$. From this order of magnitude analysis, it can be seen that the leading contribution to the dissipation rate $\mathscr{D}^{(0)}$ is identically zero, and the $O(\epsilon^{1/2})$ correction $\mathscr{D}^{(1)}$ is due to the dissipation in the viscous wall layer

$$\mathscr{D}^{(1)}(k) = 2\Gamma \int_0^\infty dy(\partial_y \tilde{v}_{wx}\, \partial_y \tilde{v}_{wx}^*) = 2\Gamma^{1/2} A_i A_i^* \frac{(s^{(0)})^{1/2}(s^{(0)*})^{1/2}}{(s^{(0)})^{1/2} + (s^{(0)*})^{1/2}}. \tag{3.6}$$

In the above expression, $r = 1 - \epsilon^{1/2}y$ and the upper limit $y = \epsilon^{-1/2}$ has been approximated by $y = \infty$. The dissipation in the outer flow in the fluid and the wall material only contributes to the $O(\epsilon)$ correction to the dissipation rate $\mathscr{D}^{(2)}$, which is not considered here.

The contribution to the rate of change of energy due to the Reynolds stresses, $\mathscr{C}$, is (Chandrasekhar 1981)

$$\mathscr{C} = -\int dx \int_0^1 r\, dr v_r v_x \partial_r \bar{v} = (2\pi)^{-1} \int dk\, \exp[2(s+s^*)t]\,\mathscr{C}(k), \tag{3.7}$$

where the spectrum of the convective transport, $\mathscr{C}(k)$, is

$$\mathscr{C}(k) = \int_0^1 r\, dr(2\Gamma r)(\tilde{v}_r \tilde{v}_x^* + \tilde{v}_r^* \tilde{v}_x). \tag{3.8}$$

The convective transport is restricted to the velocity fluctuations in the fluid, since the mean velocity in the solid is zero. It can be easily verified that the convective transport $\mathscr{C}^{(0)}(k)$ due to the leading-order velocity field $\tilde{v}^{(0)}$ is zero, because the product $\tilde{v}_{or}^{(0)} \tilde{v}_{ox}^{(0)}$ is imaginary from (2.21) and (2.22). Similarly, the $O(\epsilon^{1/2})$ contribution to the convective transport is zero because $\tilde{v}_{or}^{(1)} = 0$ and $\tilde{v}_{ox}^{(1)} = 0$ (see (2.25)). However, there is a contribution to $\mathscr{C}^{(1)}$ due to the flow in the wall layer

$$\mathscr{C}^{(1)}(k) = 2\Gamma \int_0^\infty dy(\tilde{v}_{or}^{(0)} \tilde{v}_{wx}^* + \tilde{v}_{or}^{(0)*} \tilde{v}_{wx}) = 2\Gamma^{3/2}\left[\tilde{v}_{or}^{(0)}\left(\frac{\tilde{v}_{wx}}{(s^{(0)})^{1/2}} + \frac{\tilde{v}_{wx}^*}{(s^{(0)*})^{1/2}}\right)\right]\bigg|_{r=1}. \tag{3.9}$$

In deriving the second expression, (2.30) has been used for $\tilde{v}_{wx}$, and $\tilde{v}_{or}^{(0)}$ is assumed to be a constant over a distance $O(\epsilon^{1/2})$ where $\tilde{v}_{wx}$ is non-zero; the error due to this approximation is $O(\epsilon^{1/2})$ smaller than the terms retained.

The deformation work done by the stresses at the bounding surfaces of the fluid and the wall, $\mathscr{S}$, is (Chandrasekhar 1981)

$$\mathscr{S} = \int dS_i\, \sigma_{ij} v_j, \tag{3.10}$$

where dS_i is an area element of the bounding surface directed along the outward normal to the surface. The work done on the wall material at $r = H$ is zero because the normal and tangential velocities are zero at this surface. At the interface $r = 1$, the work done on the fluid is given by

$$\mathscr{S}_f = \int dx(\tau_{rr} v_r + \tau_{xr} v_x), \tag{3.11}$$

while the work done on the wall material is

$$\mathscr{S}_s = -\int dx(\sigma_{rr} \partial_t u_r + \sigma_{xr} \partial_t u_x). \tag{3.12}$$

There is a negative sign in the above equation because the outward normal is directed along the $-r$-direction. The total work done at the surface is the sum of (3.11) and (3.12). Since the normal velocity and stress are continuous across the interface, the net work done by the normal stresses in (3.11) and (3.12) cancel. Physically, this implies that there is a transfer of energy between the fluctuations in the fluid and wall due to the normal stresses, but there is no net transport of energy from the mean flow. The shear stress is also continuous at the interface, but there is a discontinuity in the tangential velocity, which is proportional to $(2\Gamma u_r)$ (see (2.16)). The net work done by the shear stresses at the interface is

$$\mathscr{S} = \int dx \tau_{xr}(v_x - \partial_t u_x) = (2\pi)^{-1} \exp\left[(s + s^*)\,t\right] \int dk \mathscr{S}(k), \tag{3.13}$$

where the spectrum of the deformation work $\mathscr{S}(k)$ is obtained by inserting (2.9) into (3.13):

$$\mathscr{S}(k) = [2\Gamma(\tilde{\tau}_{xr} \tilde{u}_r^* + \tilde{\tau}_{xr}^* \tilde{u}_r)]. \tag{3.14}$$

Here, (2.16) has been used for the discontinuity in the velocity across the surface. Inserting (3.32) for the leading-order shear stress at the surface $\tilde{\tau}_{wxr}$, the final expression for the leading-order work done due to the surface stresses is

$$\mathscr{S}(k) = 2\epsilon^{1/2}\Gamma^{3/2}[(s^{(0)})^{1/2}\tilde{v}_{wx}\,\tilde{u}_r^{(0)*} + (s^{(0)*})^{1/2}\tilde{v}_{wx}^*\,\tilde{u}_r^{(0)}]|_{r=1}$$

$$= -2\epsilon^{1/2}\Gamma^{3/2}\left[\tilde{v}_{or}^{(0)}\left(\frac{\tilde{v}_{wx}}{(s^{(0)})^{1/2}} + \frac{\tilde{v}_{wx}^*}{(s^{(0)*})^{1/2}}\right)\right]\Bigg|_{r=1}, \tag{3.15}$$

where the normal velocity condition (2.38) was used to obtain the second expression. From (3.15), it can be seen that $\mathscr{S}^{(0)} = 0$, and

$$\mathscr{S}^{(1)}(k) = -2\Gamma^{3/2}\left[\tilde{v}_{or}^{(0)}\left(\frac{\tilde{v}_{wx}}{(s^{(0)})^{1/2}} + \frac{\tilde{v}_{wx}^*}{(s^{(0)*})^{1/2}}\right)\right]\Bigg|_{r=1}. \tag{3.16}$$

The above calculations indicate that $\mathscr{D}^{(0)}$, $\mathscr{C}^{(0)}$ and $\mathscr{S}^{(0)}$ are all identically zero, and from (3.3) it can be inferred that the real part of $s^{(0)}$ is zero. This is in agreement with the results of the linear stability analysis of the previous section. In addition, a comparison of (3.9) and (3.16) shows that $\mathscr{S}^{(1)}(k) + \mathscr{C}^{(1)}(k) = 0$, i.e. the rate of

transport of energy due to the deformation work at the surface is exactly the negative of the rate of transport of energy in the wall layer due to the Reynolds stresses. This general feature of the wall layer flow near a flexible surface, which does not appear to have been noticed before, is just a consequence of the continuity of velocity and stress conditions at the surface. In the absence of any net energy transport, the dissipation $\mathcal{D}^{(1)}$ in the wall layer causes the damping of the fluctuations, and therefore $s^{(1)}$ is always negative. However, it was found in the previous section that $s^{(1)} = 0$ at certain points in the Γ, k parameter space. This is because the amplitude of the wall layer velocity $\tilde{v}_{wx}$ becomes zero at these points, and the tangential velocity boundary condition is identically satisfied by the outer flow. At these points the decay rate of the perturbations, which is $O(\epsilon)$ smaller than the frequency, is determined by the relative magnitudes of the dissipation rate in the outer flow and wall material, and the deformation work done by the outer flow shear stresses at the interface.

We end this section with a brief discussion of the behaviour of $s^{(1)}$ in the limit $k \gg 1$ (figure 5). The decay of the fluctuations is due to the dissipation in the wall layer in the fluid, and not due to the dissipation in the bulk of the fluid or wall material. If the normal velocity fluctuation at the surface scales as $\tilde{v}$, then the normal displacement at the surface is $O(\tilde{v}/s^{(0)})$. However, the incompressibility condition (2.13) stipulates that $\partial_r \tilde{u}_r \sim k \tilde{u}_x$, and therefore the displacement field in the bulk of the wall material is $O(k\tilde{v}/s^{(0)})$, which is $O(\tilde{v})$ since $s^{(0)} \propto k$ for $k \gg 1$. The elastic energy then scales as $k^2 \tilde{v}^2$, which is of the same magnitude as the kinetic energy of the wall motion. The kinetic energy in the fluid scales as $k^{-1} \tilde{v}^2$, which is $O(k^{-1})$ smaller than what one might expect from a naive scaling argument because the penetration depth of the fluctuations in the fluid at large k is $O(k^{-1})$. The rate of dissipation of energy in the wall layer increases proportional to $(s^{(0)})^{1/2}$ from (3.6), and therefore the decay rate for the second and higher harmonics decreases proportional to $k^{-3/2}$ for $k \gg 1$.

The decay rate for the first harmonic has a different trend for the following reason. Detailed calculations indicate that the eigenvalue γ in (2.33) and (2.34) is real for the first harmonic, and the strain field in the wall material is confined to a region of thickness $O(k^{-1})$ at the surface. Moreover, the amplitude of the displacement field in this region is $O(\tilde{v}/s^{(0)})$, and consequently the strain energy decreases $\propto k^{-1} \tilde{v}^2$ for $k \gg 1$. The kinetic energy in the fluid and the wall exhibit a similar trend, and therefore the first correction to the growth rate increases proportional to $k^{3/2}$ for $k \gg 1$. Therefore, the difference in the behaviour of the first and the higher harmonics is caused by the difference in the qualitative nature of the strain field in the wall. A similar trend is also observed for the second correction to the growth rate $s_1^{(2)}$ (figure 8*a*), which is a consequence of the dissipation in the outer flow. The contribution $s_2^{(2)}$ due to the dissipation in the wall material (figure 8*b*) shows the expected increase proportional to k^2.

4. Conclusions

The stability of the high Reynolds number flow in a tube with flexible walls was analysed in this paper. The present system is qualitatively different from the flow in a tube with rigid walls at high Reynolds number. An inviscid Hagen–Poiseuille flow in a tube with rigid walls does not have any unstable or neutrally stable solutions because there are no points of inflexion in the flow as required by the Rayleigh theorem. In fact, a stronger statement can be made that the temporal stability problem for an inviscid flow in a rigid tube does not have any solutions. Further, there are no solutions at high Reynolds number that involve an inner critical layer, as in the case of the flow in a two-

dimensional channel. The flow in a flexible tube is not constrained by the Rayleigh theorem because a normal velocity is permitted at the wall. Therefore, an inviscid flow in the present configuration does have non-trivial solutions, and an asymptotic analysis about the inviscid flow was used in the present study. The growth rate of the fluctuations was determined using a linear stability calculation, and an energy balance analysis was employed to obtain some physical insight into the energy transport processes in the system.

The system consisted of a tube of radius R surrounded by a viscoelastic medium in the annular region $R < r < HR$. The fluid was considered to be an incompressible Newtonian fluid, while the wall was modelled as an incompressible viscoelastic medium in which the stress has an elastic component proportional to the strain and a viscous component proportional to the strain rate. The dynamics of the system is influenced by four dimensionless parameters – the Reynolds number $Re = (\rho VR/\eta)$, the ratio of radii H, the ratio of the viscosities of the wall material and fluid $\eta_r = (\eta_s/\eta)$ and the dimensionless velocity $\Gamma = (\rho V^2/G)^{1/2}$. In the high Reynolds number limit, an asymptotic expansion in the small parameter $\epsilon = (1/Re)$ was used.

In the leading approximation, the flow is inviscid, and it is observed that the leading-order growth rate $s^{(0)}$ is imaginary, indicating that the perturbations are neutrally stable at this level of approximation. This is because there is neither viscous dissipation of energy nor any transport of energy from the mean flow to the fluctuations due to Reynolds stress. There are multiple solutions for the leading-order frequency, and it is found that an increase in the fluid velocity tends to increase the frequency of the downstream travelling waves and decrease the frequency of the upstream travelling waves.

The viscous stresses are $O(\epsilon^{1/2})$ smaller than the inertial stresses in the fluid in a wall layer of thickness $O(\epsilon^{1/2}R)$ at the interface. As a consequence of the wall layer, there is an $O(\epsilon^{1/2})$ correction $s^{(1)}$ to the leading-order frequency. This correction does not depend on the viscosity of the wall material because the damping is due to the energy dissipation in the wall layer and not in the bulk of the fluid or the wall. In the wall layer, it was found that the transfer of energy from the mean flow to the fluctuations due to the Reynolds stress is cancelled by the opposite transfer of equal magnitude due to the deformation work done by the shear stress, resulting in no net transport of energy to the velocity fluctuations. This is a general result for the flow in a wall layer near a flexible surface, which does not appear to have been reported earlier. As a result, the dissipation in the wall layer has a stabilizing effect on the fluctuations, and the real part of the $O(\epsilon^{1/2})$ correction to the growth rate $s^{(1)}$ is negative. An increase in the fluid velocity tends to stabilize the upstream travelling waves, and destabilize the downstream travelling waves.

There are certain parameter values (Γ_c, k_c) where it is found that $s^{(1)} = 0$ for the downstream travelling waves. This is a rather interesting feature which does not seem to have been observed in previous studies. Physically, this feature occurs because the amplitude of the wall layer velocity becomes zero at these points, and the tangential velocity boundary condition is identically satisfied by the inviscid flow. At these points, the stability is determined by the $O(\epsilon)$ correction to the growth rate $s^{(2)}$. It was found that $s^{(2)}$ does depend on η_r because the viscous effects in the bulk of the fluid and the wall are important at this level of approximation. The real part of $s^{(2)}$ was found to be negative along the curves (Γ_c, k_c) where $s^{(1)} = 0$, indicating the presence of a small stabilizing effect. The variation of the minimum of $s^{(2)}$ as a function of H was examined, and it was found that the minimum value increases proportional to $(H-1)^{-2}$ for $(H-1) \ll 1$, and decreases proportional to H^{-4} for $H \gg 1$.

The oscillations in the present system correspond most closely to the Class B waves in the classification of Benjamin (1963). These are waves which involve a conservative exchange of energy between the fluid and the solid, and the energy dissipation in the fluid or solid tends to dampen the fluctuations. They also exhibit another distinctive feature of Class B waves – the ability to propagate even in the absence of a fluid. The present analysis has not revealed any Class A type waves, which are destabilized by dissipation in the solid. In addition, we have also not observed any Class C (Kelvin–Helmholtz) type waves. In the classification scheme of Carpenter & Garrad, these could be included in the flow-induced surface wave category, which could exist even in the absence of fluid viscosity.

It is useful to compare the present results with those of the high Reynolds number asymptotic analysis in a rigid tube. In a rigid tube, no-slip conditions are enforced at the wall and there are no non-trivial solutions of the inviscid equations of motion. There are, however, solutions of the complete Navier–Stokes equations where the vorticity is important in a thin region near the centre of the tube or the wall. A complete discussion of these modes is given in Davey & Drazin (1969) and Drazin & Reid (1981). There are two types of viscous modes at high Reynolds number:

(i) the 'centre modes', where the vorticity is important in a region of thickness $(kRe)^{-1/4}$ near the centre of the tube: the damping rate of these modes is proportional to $(kRe)^{-1/2}$ when scaled by (V/R), but the leading-order wave speed is 1 when scaled by the mean velocity, indicating that the perturbations are travelling at the same velocity as the fluid;

(ii) the 'wall modes' where the vorticity is confined to a region of thickness $(kRe)^{-1/3}$ near the wall: both the frequency and the damping rate of these modes is proportional to $(kRe)^{-1/3}$.

It might be expected that the damping rate for the centre modes in a flexible tube will be the same as that for a rigid tube in the leading-order approximation. This is because the vorticity is confined to a region small compared to the radius of the tube, and is insensitive to the boundary condition applied at the wall. However, it can be shown that the leading-order damping rate for the wall modes is also unaffected by the flexibility of the wall, because the boundary condition at the wall is identical to the no-slip condition for a rigid tube in the leading approximation. If the fluctuation in the velocity at the wall is $O(v)$, the shear stress scales as $(Re^{1/3}\eta v/R)$ since the thickness of the wall layer is $O(Re^{-1/3}R)$. This is balanced by the elastic stress in the wall material, which is $O(Gu/R)$ where u is the magnitude of the displacement. A balance between these two stresses indicates that $u \sim Re^{1/3}(\eta v/G)$. The magnitude of the velocity of the wall material at the surface, $\partial_t u_i$, scales as $(Re^{-1}\Gamma^2 v)$, because the frequency of the oscillations is $O(Re^{-1/3}V/R)$ for the wall modes. For the present regime where $Re \gg 1$ and $\Gamma \sim 1$, this is equivalent to a no-slip condition in the leading approximation, and consequently the leading-order damping rate for the wall modes is the same as that for a rigid wall.

The damping rates of the inviscid modes in the present analysis is $O(Re^{-1/2})$ lower than the leading-order frequency for $\Gamma \sim 1$. This is lower than the $O(Re^{-1/3})$ damping rate for the wall modes, and is of the same magnitude as the $O(Re^{-1/2})$ damping rates for the centre modes. However, we find certain parameter values where the damping rate is $O(Re^{-1})$ lower than the leading-order frequency, which is lower than even the damping rate of the centre modes, and these inviscid modes are the least-damped modes in the flow through a flexible tube. The small damping rates of these fluctuations is due to the presence of a resonance-like mechanism at these parameter values, where the tangential velocity boundary condition is identically satisfied by the inviscid

solution. In this case, there is no boundary layer near the wall, and the damping due to the viscous dissipation in the bulk of the flow is $O(Re^{-1})$. This mechanism is facilitated by the flexibility of the wall, which acts as a destabilizing mechanism in this case.

Though no instabilities were observed in the present analysis, the presence of slowly decaying modes with decay rate $O(1/Re)$ smaller than the leading-order frequency were detected for certain parameter values. Further, it was found that the minimum decay rate decreases proportional to H^{-4} when the ratio of radii H becomes large. The presence of these slowly decaying fluctuations could have a significant effect on the transport processes in these flows. Further, this could be important in biological flows which are driven by an oscillating pressure drop. The earlier analysis of the viscous flow through a flexible tube (Kumaran 1995) revealed the presence of instabilities when the velocity is increased beyond a critical value. Though the two studies are not directly comparable, because that analysis considered the regime $(\eta V/GR) \sim O(1)$ while the present one assumes $(\rho V^2/G)^{1/2} \sim O(1)$, it is still surprising that an increase in the Reynolds number appears to have a stabilizing effect. The instability at low Reynolds number is due to the transport of energy from the mean flow to the fluctuations due to the deformation work done by the mean flow at the interface. At high Reynolds number, the transfer of energy due to the deformation work is cancelled by an opposite transfer of energy due to Reynolds stresses in the wall layer, and there is no net transfer of energy from the mean flow to the fluctuations. This fortuitous cancellation of the energy transfer terms gives rise to the paradoxical result that the flow at low Reynolds number could become unstable, while the flow in the limit of high Reynolds number is stable.

REFERENCES

BENJAMIN, T. B. 1959 Shearing flow over a wavy boundary layer. *J. Fluid Mech.* **6**, 161–205.

BENJAMIN, T. B. 1963 The threefold classification of unstable disturbances in flexible surfaces bounding inviscid flows. *J. Fluid Mech.* **16**, 436–450.

CARPENTER, P. W. 1990 Status of transition delay using compliant walls. *Prog. Astro. Aero.* **123**, 79–113.

CARPENTER, P. W. & GAJJAR, J. G. S. 1990 A general theory for two- and three-dimensional wall mode instabilities in boundary layers over isotropic and anisotropic compliant walls. *Theor. Comput. Fluid Dyn.* **1**, 349–378.

CARPENTER, P. W. & GARRAD, A. D. 1985 The hydrodynamic stability of flows over Kramer-type compliant surfaces. Part 1. Tollmien–Schlichting instabilities. *J. Fluid Mech.* **155**, 465–510.

CARPENTER, P. W. & GARRAD, A. D. 1986 The hydrodynamic stability of flows over Kramer-type compliant surfaces. Part 2. Flow induced surface instabilities. *J. Fluid Mech.* **170**, 199–232.

CHANDRASEKHAR, S. 1981 *Hydrodynamic and Hydromagnetic Stability*. Dover.

CORCOS, G. M. & SELLARS, J. R. 1959 On the stability of fully developed flow in a pipe. *J. Fluid Mech.* **5**, 97–112.

DAVEY, A. & DRAZIN, P. G. 1969 The stability of Poiseuille flow in a pipe. *J. Fluid Mech.* **36**, 209–218.

DRAZIN, P. G. & REID, W. H. 1981 *Hydrodynamic Stability*. Cambridge University Press.

GARG, V. K. & ROULEAU, W. T. 1972 Linear spatial stability of pipe Poiseuille flow. *J. Fluid Mech.* **54**, 113–127.

GILL, A. E. 1965 On the behaviour of small disturbances to Poiseuille flow in a circular pipe. *J. Fluid Mech.* **21**, 145–172.

GRAEBEL, W. P. 1970 The stability of pipe flow. Part 1. Asymptotic analysis for small wave numbers. *J. Fluid Mech.* **43**, 279–290.

HANSEN, R. J. & HUNSTON, D. L. 1974 An experimental study of turbulent flows over a compliant surface. *J. Sound Vib.* **34**, 297–308.

HANSEN, R. J. & HUNSTON, D. L. 1983 Fluid property effects on flow-generated waves on a compliant surface. *J. Fluid Mech.* **133**, 161–177.

HARDEN, J. H., PLEINER, H. & PINCUS, P. A. 1991 Hydrodynamic modes on concentrated polymer solutions and gels. *J. Chem. Phys.* **94**, 5208–5217.

KRINDEL, P. & SILBERBERG, A. 1979 Flow through gel-walled tubes. *J. Colloid Interface Sci.* **71**, 34–50.

KUMARAN, V. 1993 Surface modes on a polymer gel of finite thickness. *J. Chem. Phys.* **98**, 3429–3438.

KUMARAN, V. 1995 Stability of the viscous flow of a fluid through a flexible tube. *J. Fluid Mech.* **294**, 259–281.

KUMARAN, V., FREDRICKSON, G. H. & PINCUS, P. 1994 Flow induced instability at the interface between a fluid and a gel at low Reynolds number. *J. Phys. Paris (II)* **4**, 893–904.

LANDAHL, M. T. 1962 On the stability of a laminar incompressible boundary layer over flexible surface. *J. Fluid Mech.* **13**, 609–632.

LANDAU, L. D. & LIFSHITZ, E. M. 1989 *Theory of Elasticity.* Pergamon.

LIN, C. C. 1945*a* On the stability of two-dimensional parallel flows, Part 1. *Q. Appl. Maths* **3**, 117–142.

LIN, C. C. 1945*b* On the stability of two-dimensional parallel flows, Part 2. *Q. Appl. Maths* **3**, 218–234.

LIN, C. C. 1945*c* On the stability of two-dimensional parallel flows, Part 3. *Q. Appl. Maths* **3**, 277–301.

LIN, C. C. 1966 *The Theory of Hydrodynamic Stability.* Cambridge University Press.

PEKERIS, C. L. 1948 Stability of the laminar flow through a pipe of circular cross-section to infinitesimal disturbances which are symmetrical about the axis of the pipe. *Proc. US Natl Acad. Sci.* **34**, 285–295.

RILEY, J., GAD EL HAK, M. & METCALFE, R. W. 1988 Compliant coatings. *Ann. Rev. Fluid Mech.* **20**, 393–420.

SALWEN, H. & GROSCH, C. E. 1972 The stability of Poiseuille flow in a pipe of circular cross section. *J. Fluid Mech.* **54**, 93–112.

SCHLICHTING, H. 1933 Zur Entstehung der Turbulenz bei der Plattenstromung. *Z. Agnew. Math. Mech.* **13**, 171–174.

SILBERBERG, A. 1987 Physico-chemical hydrodynamics in turbulent flows close to an interface. *Physico-chem. Hydrodyn.* **9**, 419–426.

SREENIVASAN, K. R. & RAMSHANKAR, R. 1986 Transition intermittency in open flows, and intermittency routes to chaos. *Physica* **23D**, 246–258.

TOLLMIEN, W. 1929 Über die Entstehung der Turbulenz. 1. *Mitt. Ges. Wiss. Göttingen, Math. Phys. Klasse*, 21–44.

WASOW, W. 1953 Asymptotic solution of the differential equation of hydrodynamic stability in a domain containing a transition point. *Ann. Maths* **58**, 222–252.

WYGNANSKI, I. & CHAMPAGNE, F. H. 1973 On transition in a pipe. Part 1. The origin of puffs and slugs, and the flow in a turbulent slug. *J. Fluid Mech.* **59**, 281–335.